Broering et al., http://www.jcb.org/cgi/content/full/jcb.201311050/DC1

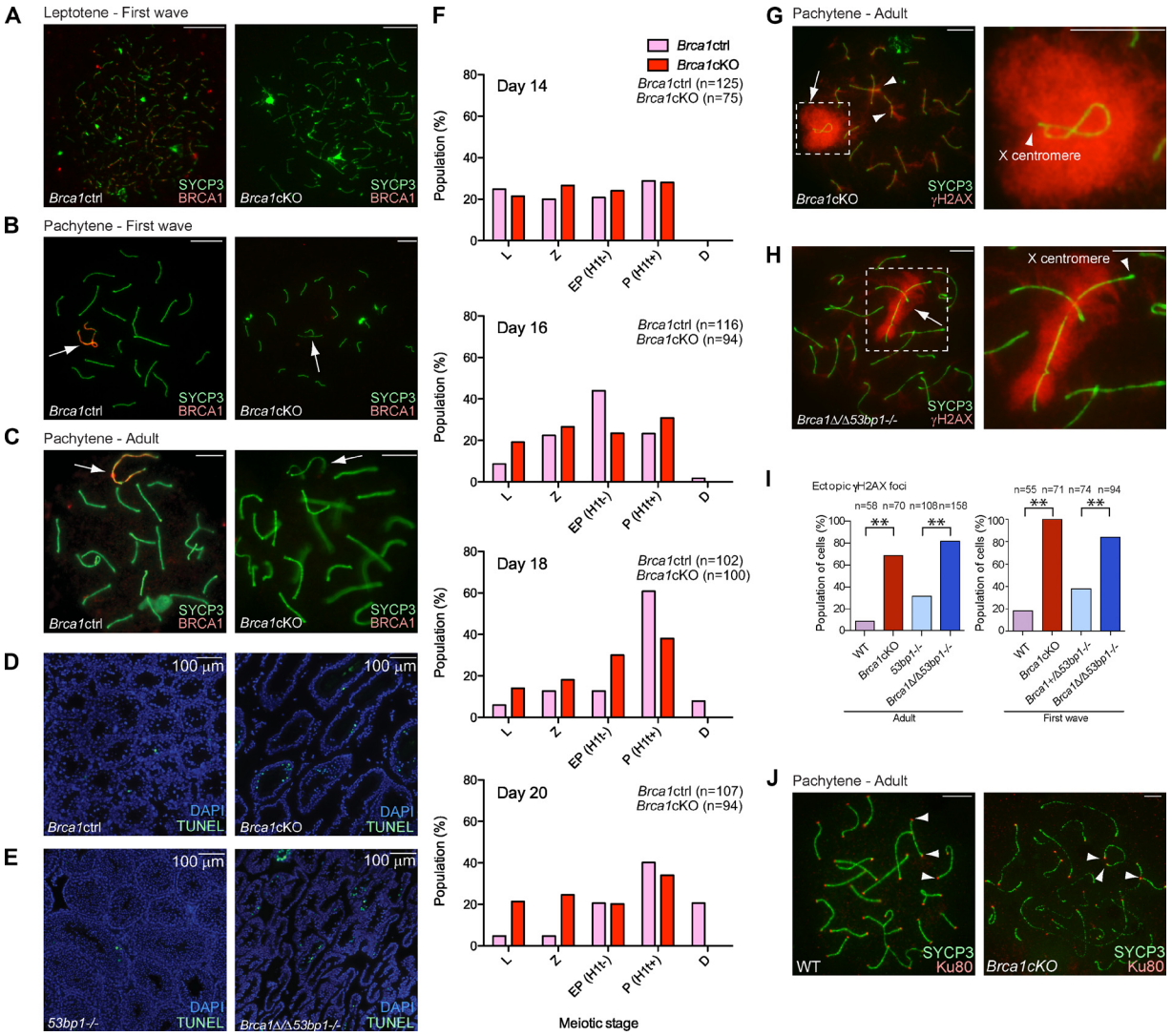

Figure S1. **Meiotic progression of *Brca1* mutants.** (A–C) Evaluation of the efficiency of conditional deletion of *Brca1*. Immunostaining of meiotic chromosome spreads using an anti-SYCP3 and -BRCA1 antibody raised against amino acids 789–1,141 (encoded by exon 11) of BRCA1. Immunostaining of first wave meiosis is shown in A and B and of adult meiosis in C. Arrows indicate sex chromosomes. (D and E) TUNEL staining of the 3-wk-old testis of the *Brca1*cKO and 4-wk-old testis of the *Brca1*Δ/Δ*53bp1*$^{-/-}$ and their littermate controls. (F) Meiotic progression of the first wave meiosis at day 14, 16, 18, and 20 of the *Brca1*cKO judged by SYCP3 and H1t double immunostaining. (G) An example of ectopic γH2AX domain formation in the *Brca1*cKO. Arrows indicate sex chromosomes. Arrowheads indicate ectopic γH2AX foci. γH2AX domain formation on the sex chromosomes appears to be complete, but the presence of γH2AX is relatively decreased in the X-pericentric region. (H) A large γH2AX domain was observed on the sex chromosomes, but it failed to spread onto the X-pericentric region. (I) The population of pachytene spermatocytes exhibiting ectopic γH2AX foci. P-values were derived from an unpaired *t* test. **, $P < 0.001$. (J) Immunostaining of meiotic chromosome spreads using anti-Ku80 and -SYCP3 antibodies. Arrowheads indicate Ku80 foci localized at the ends of synapsed chromosomes. Bars, 10 µm (except in D and E as shown).

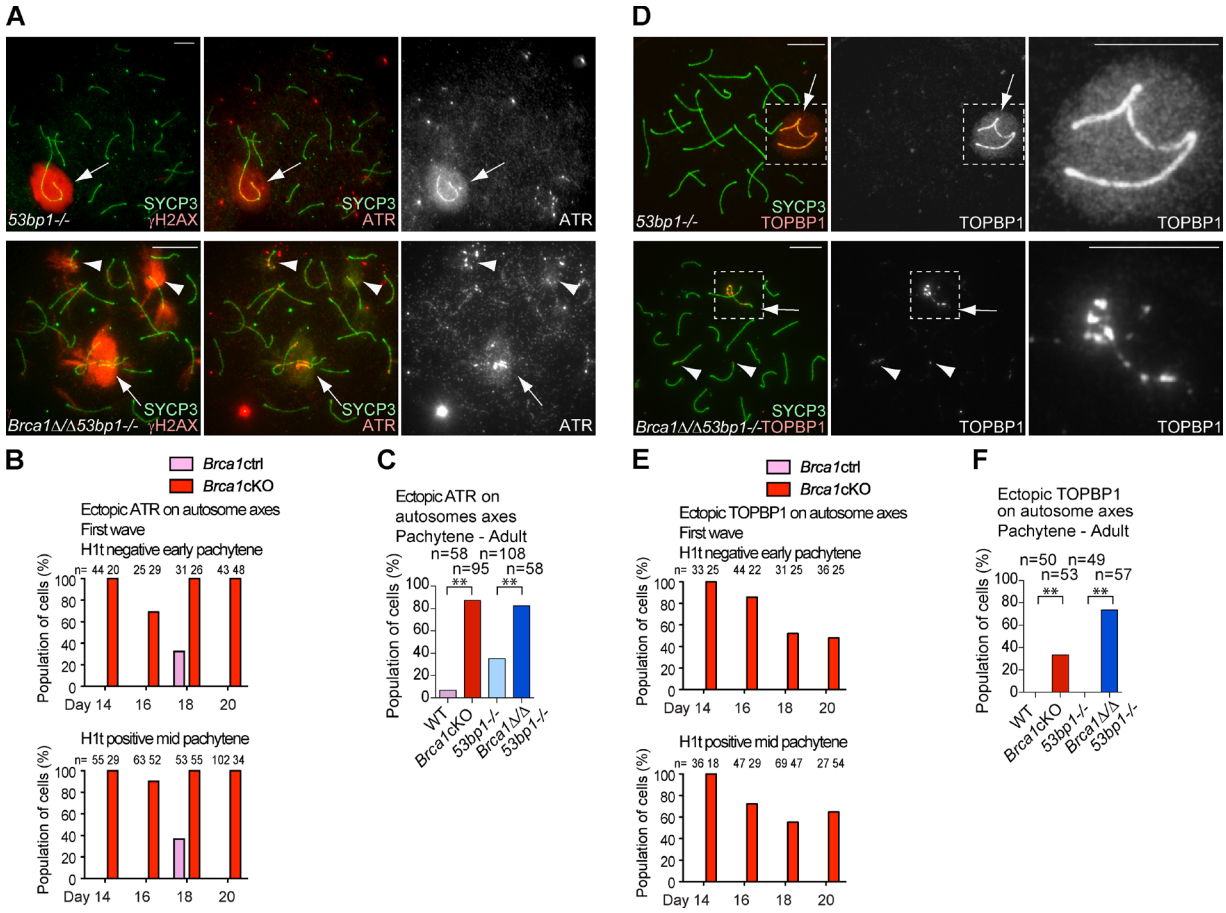

Figure S2. **Ectopic accumulation of ATR and TOPBP1 on autosome axes in *Brca1* mutants.** (A) Immunostaining of meiotic chromosome spreads of adult meiosis using anti-SYCP3, -γH2AX, and -ATR antibodies. (B and C) Percentage of pachytene spermatocytes exhibiting ectopic ATR accumulation on autosome axes in the first wave meiosis (B) and in adult meiosis (C). (D) Immunostaining of meiotic chromosome spreads using anti-SYCP3 and -TOPBP1 antibodies. (E and F) Percentage of pachytene spermatocytes exhibiting ectopic TOPBP1 accumulation on autosome axes in the first wave-meiosis (E) and in adult meiosis (F). Arrows indicate sex chromosomes. Arrowheads indicate ectopic foci on autosomes. P-values were derived from an unpaired *t* test. **, $P < 0.001$. Bars, 10 µm.

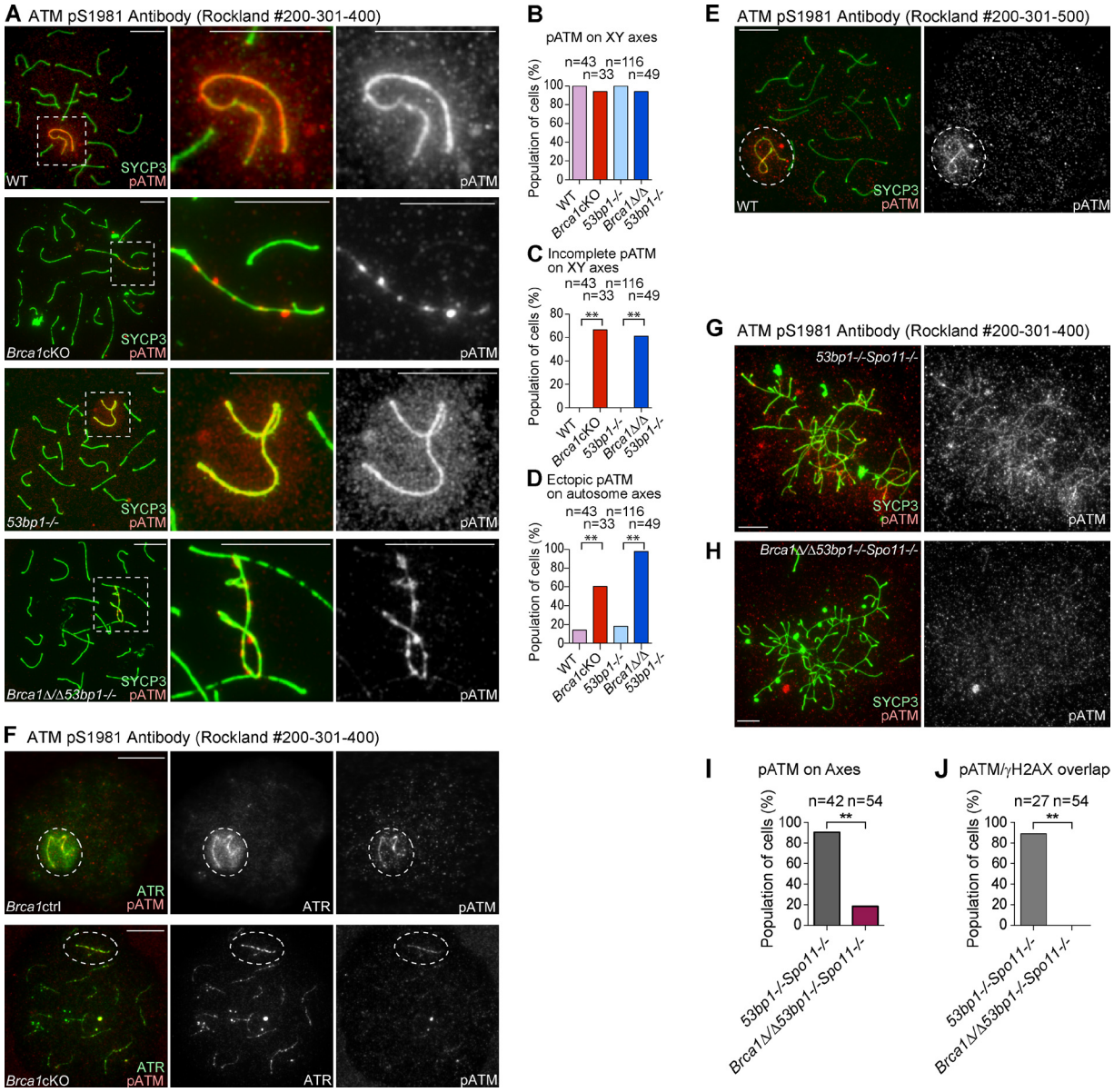

Figure S3. **BRCA1 regulates phospho-ATM in meiotic silencing.** (A) Immunostaining of meiotic chromosome spreads using anti-SYCP3 and –phospho-ATM (red; #200-301-400; Rockland) antibodies. (B) The percentage of pachytene spermatocytes exhibiting phospho-ATM foci accumulation on XY axes. (C) The percentage of pachytene spermatocytes demonstrating dispersed, punctate phospho-ATM foci on XY axes. (D) The percentage of pachytene spermatocytes exhibiting ectopic phospho-ATM foci. Phospho-ATM was intensely localized on entire XY axes and formed distinct domains surrounding the sex chromosomes in 100% of wild-type and *53bp1*$^{-/-}$ pachytene spermatocytes (A). The localization of phospho-ATM was very similar to that of TOPBP1 in both *Brca1* mutants and controls. Although phospho-ATM signals were present on the XY axes in *Brca1* mutants (A and B), 66.7% of *Brca1*cKO and 61.2% of *Brca1*Δ/Δ*53bp1*$^{-/-}$ spermatocytes demonstrated dispersed, punctate phospho-ATM localization along the XY axes and failed to establish phospho-ATM domains on the entire region of the sex chromosomes (A and C). Although phospho-ATM predominantly accumulated on the XY axes in these mutants, ectopic and dotted phospho-ATM signals were observed on portions of autosomal axes in 60.6% of *Brca1*cKO cells and 97.9% of *Brca1*Δ/Δ*53bp1*$^{-/-}$ spermatocytes (A and D). (E) The localization of phospho-ATM on the sex chromosomes was confirmed with an independent anti–phospho-ATM antibody (#200-301-500; Rockland). The area of the sex chromosomes is shown in the dotted circle. (F) ATR and phospho-ATM localize to identical sites along the X axis in Brca1cKO spermatocytes. (G–J) BRCA1 regulates phospho-ATM in ectopic meiotic silencing in a *Spo11* mutant background. (G and H) Immunostaining of meiotic chromosome spreads using anti–phospho-ATM and SYCP3 antibodies. (I) Population distribution of phospho-ATM on axes in pachytene-like spermatocytes. (J) Population distribution of cells with overlap of γH2AX and TOPBP1 in pachytene-like spermatocytes. Phospho-ATM signals were observed on chromosome axes in 90.0% of pachytene-like spermatocytes of *53bp1*$^{-/-}$*Spo11*$^{-/-}$ mice (G and I), but the axial phospho-ATM signals were observed in only 18.5% of pachytene-like spermatocytes of *Brca1*Δ/Δ*53bp1*$^{-/-}$*Spo11*$^{-/-}$ mice (H and J). Furthermore, phospho-ATM signals never overlapped with γH2AX in *Brca1*Δ/Δ*53bp1*$^{-/-}$*Spo11*$^{-/-}$ spermatocytes despite the colocalization of phospho-ATM and γH2AX in 88.9% of *53bp1*$^{-/-}$*Spo11*$^{-/-}$ cells (J). P-values were derived from an unpaired *t* test. **, P < 0.001. Bars, 10 μm.

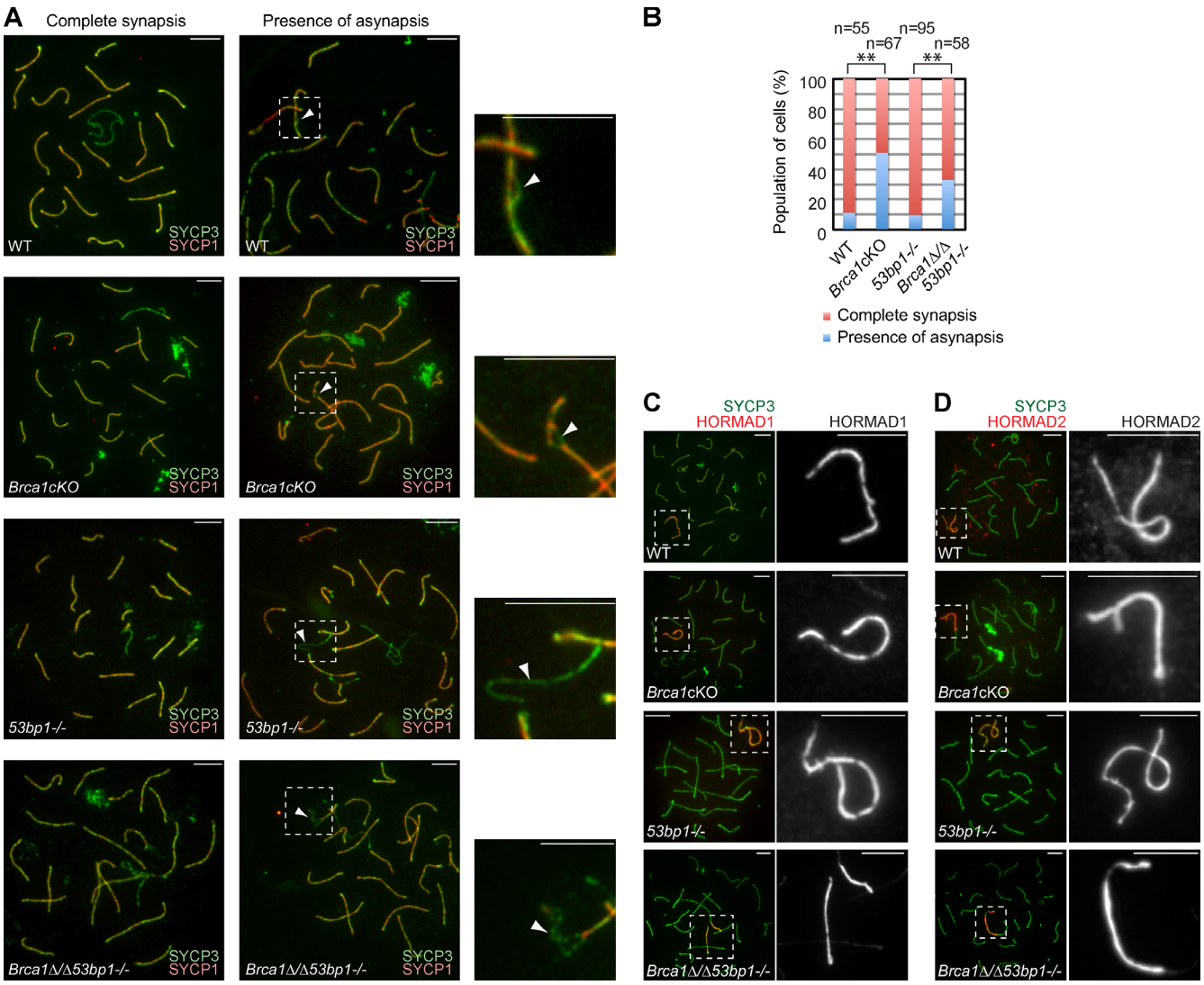

Figure S4. **Autosomal asynapsis in *Brca1* mutants.** (A) Autosomal asynapsis was detected by immunostaining meiotic chromosome spreads using anti-SYCP3 and -SYCP1 antibodies. The SYCP1 antibody recognizes synapsed chromosome axes. Left panels are examples of complete synapsis and right panels are examples of the presence of autosomal asynapsis in at least one region in a nucleus. Arrowheads indicate regions of autosomal asynapsis. (B) The percentage of pachytene spermatocytes exhibiting complete synapsis or the presence of autosomal asynapsis from mice of the indicated genotypes. (C and D) Immunostaining of meiotic chromosome spreads using anti-HORMAD1, -HORMAD2, and -SYCP3 antibodies. P-values were derived from an unpaired *t* test. **, $P < 0.001$. Bars, 10 µm.

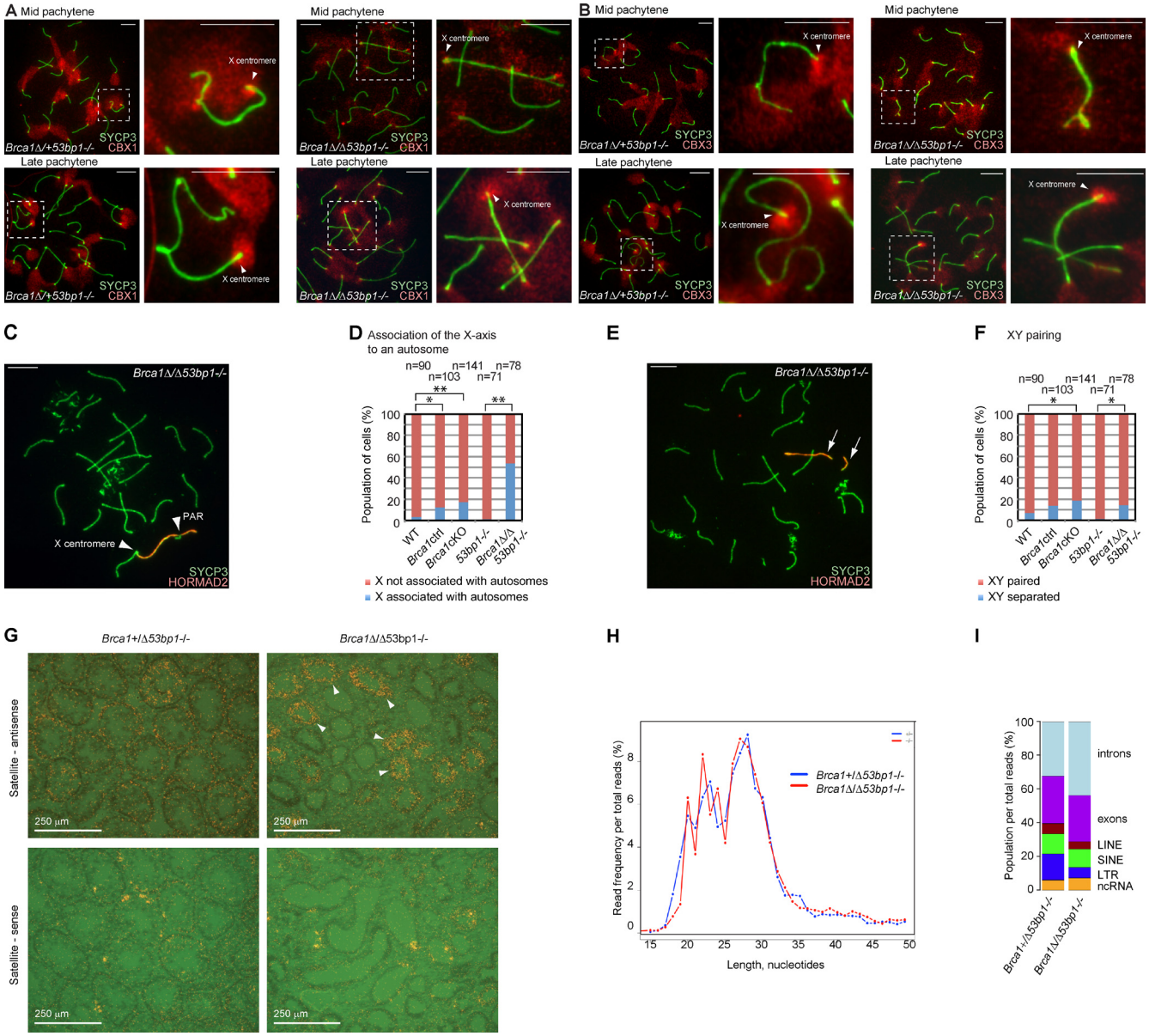

Figure S5. **BRCA1 does not regulate heterochromatin proteins on the X-PCH but regulates satellite DNA and LTR.** (A and B) Immunostaining of spermatogenesis slides that preserve intact chromatin conformation using an anti-CBX1 (A) and an anti-CBX3 antibody (B). In the mid-pachytene stage, the *Brca1* mutant signal intensities of CBX1 and CBX3 on the X-pericentric regions are relatively lower than that of the controls. However, at the late pachytene stage, both CBX1 and CBX3 highly accumulate on the X-pericentric region, both in controls and in *Brca1* mutants. (C) Association of the X axis to an autosome was detected by immunostaining meiotic chromosome spreads using anti-SYCP3 and -HORMAD2 antibodies. (D) Population of pachytene spermatocytes exhibiting association of the X axis to an autosome. (E) Separation of X and Y axes was detected by immunostaining meiotic chromosome spreads using anti-SYCP3 and -HORMAD2 antibodies. Arrows indicate sex chromosomes. (F) The population of pachytene spermatocytes exhibiting separation of X and Y axes. (G) In situ hybridization of satellite transcripts using testicular sections. Arrowheads indicate tubules with germ cells in *Brca1Δ/Δ53bp1*$^{-/-}$ testes. (H) Distribution of read length (nucleotides) of small RNA sequencing. Read frequency per total reads (percentage) is shown. (I) Percentage of each genomic element per total reads. In addition to genomic elements shown in the panel, microRNA and satellite DNA–derived small RNAs were calculated. However, the totals of these small RNAs were very low (<0.2% for miRNA and <0.03% for satellite DNA–derived small RNAs) and not shown in the figure. P-values were derived from an unpaired *t* test. *, P < 0.05; **, P < 0.001. Bars, 10 μm (except in G as shown).